International Journal of Latest Engineering Research and Applications (IJLERA) ISSN: 2455-7137

Volume – 08, Issue – 05, May 2023, PP – 37-54

Effect of Rail Surface Roughness on Wheel Wear

Brighton N. Chirukamare[1], Tian Jianhui[2], Irene K. Agbenu[3], Dong Xiaole[4], Yang Qi[5]

(School of Mechatronic Engineering, Xi'an Technological University, Xi'an, 710021, P.R. China)

Abstract: The paper focuses on investigating the impact of rail surface roughness on wheel wear in train systems. The roughness of the rail surface is affected by various factors, and it has been observed to cause mechanical and thermal stresses that affect the wear and tear of train wheels. Severe wheel tread wear can cause a variety of problems, including increased running resistance, vehicle instability, and derailment. To solve these problems effectively, various assumptions are often made, such as the non-influence of surface roughness and heat generated during the contact. However, these assumptions could lead to an increase in unaccounted internal and external forces during the wheel-rail interaction, thereby increasing the wheel wear rate. Therefore, this paper aims to closely examine the impact of wheel-rail contact problems caused by the presumption of non-influence of surface roughness.

Keywords: Rail surface roughness, Wheel wear, Rail surface measurement, Contact vibration

1. Introduction

The economic growth of every nation depends on effective transportation. The integration of the logistics industry has grown in significance across the globe as the rail system has emerged as one of the primary modes of transportation. Wheel-rail interactions are the main reason why railway wheels are continuously exposed to wear and rolling contact fatigue. In high-speed trains and subway systems, problems with wheel-rail wear, particularly circular wheel wear and hollow tread wear, have become a serious problem. Severe wheel tread wear reduces the stability of the vehicle, increases the height of the wheel flange, and increases running resistance. In the worst situation, it may lead to derailment. In order to restore the original profile of the flange and thread, a wheel that has been worn down or damaged needs to be reprofiled. The cost of reprofiling is increased by the fact that more metal is usually removed from the tread surface during cutting than is lost to wear. As a result, numerous studies have been carried out in an effort to determine how low-cost reprofiling might be done successfully.

In the last decade, [1]analyzed and explained the characteristics, implications, causes, and countermeasures of wheel wear on Chinese high-speed trains. Researchers have hypothesized four different types of wheel polygonal wear mechanisms so far: (1) Surface roughness of the wheel-rail induces resonance of the wheel when it rolls over it. This resonance causes a shift in the wheel and rail's frictional work, causing wheel polygonal wear [2]–[5]. (2) Wheel polygonal wear is caused by the self-excited vibration of a wheel set-track system [6]. (3) At high speeds, the center-of-gravity offset of the wheel set causes resonant vibration, which causes polygonal wheel wear [7]; (4) The initial polygon of the wheel (initial non-circular) induces to resonate, causing wheel polygonal wear[8]. These four types of wheel wear processes can partially explain some wheel polygonal wear phenomena. However, they fall short of fully explaining all wheel wear patterns on high-speed trains around the world.

Numerous effective countermeasures against the development of rail wheel wear have been developed, but no conclusion has been reached. Much research has been focusing on rail material properties and operating conditions such as speed and environmental weather but wheel-rail contact wear problem is still an issue. Recently, several research studies have used physical, mathematical, and simulation systems to investigate the mechanism of wheel wear. Many presumptions are often made in order to properly handle the wheel-rail contact problem using simulations, such as the non-influence of surface roughness and the non-influence of heat created on the contact. Rail surface roughness measurement sensors are very expensive. Wootae J[9] points out that measurement sensors are not completely accurate enough to assess all the rail surface roughness accurately hence a relatively cheaper method to analyse these presumptions will be a benefit to this research field. Figure 1 below shows the Auto Rail Checker (ARCer), one of the sensors used to measure acoustic roughness of the operating rail track surface. This sensor was used to measure longitudinal rail acoustic roughness on two rail tracks with different rail surface characteristics.

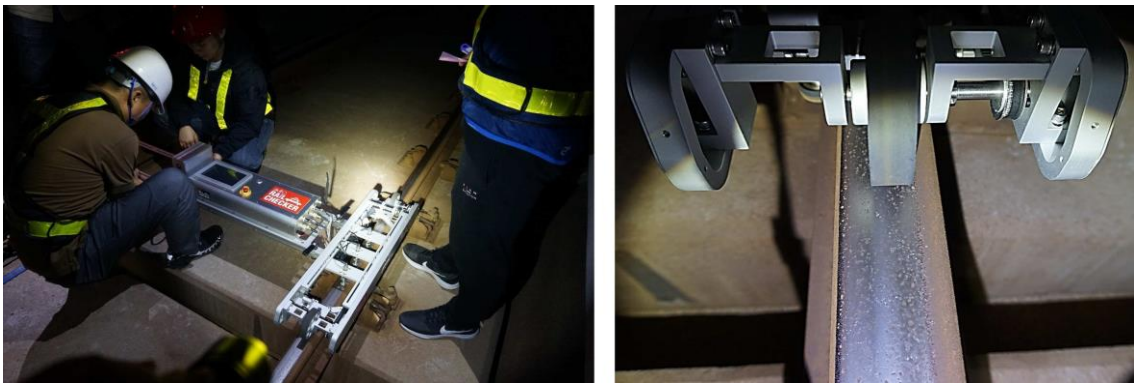

(a) Device setup (b) operating wheel and railhead

Figure 1. Field measurement of the track A; [source: [10]]

Rail acoustic roughness can be measured using a variety of transportable measurement equipment. A displacement sensor fixed to a platform that is typically positioned on a trolley-type movable measurement system [11] or an acceleration sensor installed on a mobile platform[12]is used to measure the roughness of rail surfaces. The use of a permanent system mounted on a rail to move non-contact sensors, like a laser displacement sensor, is another technique. In order to address the structural issues with mobile measuring systems equipped with displacement sensors, new techniques, such as the chord offset synchronizing method, have recently been proposed and used [10].

The roughness of the rail is defined as the deviation of the actual surface from an ideal flat surface and can be caused by factors such as corrosion, deformation, and wear resulting from the wheel-rail interaction [13], [14]. Studies have shown that the surface roughness of the rail plays a significant role in determining the wheel wear rates. High roughness values of the rail result in higher contact forces between the wheel and the rail, leading to increased wear rates [15]. Furthermore, the effect of rail surface roughness on the wear of the wheel is not limited to the contact forces alone. The roughness of the rail can also affect the lubrication conditions at the wheel-rail interface, thereby affecting the frictional forces and wear rates [16].There has been a significant growth in urban rail transit and operating speed in recent decades, which necessitates for greater research to address the problem of wheel wear.

Thus, the main area of focus of the paper is the development of numerical simulations and experimental measurements to characterize the effect of surface roughness on the wear forces of the train wheels. Ultimately, this research can contribute to the improvement of rail transportation efficiency, safety, and sustainability.

2. Methodology

This study aims to analyse the wear of train wheels at various levels of rail surface roughness. The effect of rail surface roughness on the development and advancement of wheel wear forces was evaluated using Abaqus simulation data. The simulation setup consisted of a full-size wheel set and multiple rail sets, and a high-speed contact simulation test was conducted. The Python language script in the Abaqus interface was used to vary the rail surface roughness. The wheel-rail contact wear forces were then analysed and compared for eight different rails with varying surface roughness levels. To assess the wear rate, the wear contact forces were analysed using Archard's wear model. This study aims to analyse the wear of train wheels at various levels of rail surface roughness. The effect of rail surface roughness on the development and advancement of wheel wear forces was evaluated using Abaqus simulation data. The simulation setup consisted of a full-size wheel set and multiple rail sets, and a high-speed contact simulation test was conducted.

2.1 Wear depth Model

The wear depth of train tracks depends on several factors, including the length of the track irregularities, rail hardness [17], the speed and weight of the trains, the materials used in the tracks, and the environmental conditions in which the tracks are located. Assuming that we are looking at standard gauge tracks made of steel, the wear depth can be estimated using the following formula:

$$\text{Wear depth} = \left(k * v * L * D * N\right) / \left(C * E\right) \quad (1)$$

Where, k is a constant that depends on the type of track and the materials used, v is the speed of the train in km/h, L is the length of the irregularities in meters, D is the running distance in km, N is the number of axles

per train, *C* is the hardness of the track material, and *E* is the modulus of elasticity of the track material respectively [18]. The values of *k*, *C*, and *E* will vary depending on the specific type of track and materials used, but can be estimated based on industry standards and previous studies.

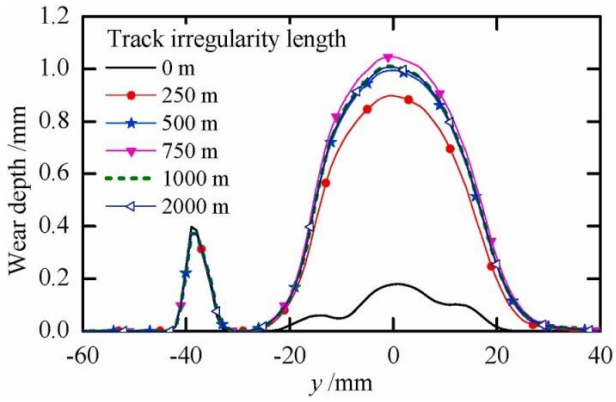

Figure 2. The wear depth with various lengths of track irregularities [source:[19]]

Assuming a typical speed of 80 km/h, a range of irregularity lengths from 5 mm to 50 mm, and a standard number of axles per train of 8, we can estimate the wear depth for a running distance of 250,000 km [19]. For irregularity length of 5 mm, where $k = 0.01$, $C = 230$, and $E = 210$ GPa:

$$\text{Wear depth} = \left(0.01*80*0.005*250000*8\right)/\left(230*210\text{GPa}\right) \quad (2)$$

It is important to note that these are just rough estimates and actual wear depth will depend on many variables that are difficult to predict with accuracy. Additionally, regular maintenance and repair of the tracks can help to mitigate wear and prolong the life of the track.After running 250,000 km with various lengths of track imperfections, Figure 2illustrates the wear depth dispersed in the lateral direction of the wheel profile. The wear depth on the wheel tread is significantly smaller than in the other scenarios when track irregularities are not considered. Furthermore, when the length of the irregularities exceeds 500m, the predicted wear is much less sensitive to the length of the irregularities. Since the detected irregularities vary along the track for some railway lines, a longer excitation may be used in some simulations.

The rail's wheel roughness affects the creation of wheel wear. Using a railway track model, from [20] it can be observed that the vibration level on the left wheel was lower than the right wheel in a polygonal wear simulation in the lab. This is because the left track wheel had just been newly ground prior to the test, giving it a smoother surface. As a result, the left wheel had significantly less excitation than the right, and polygonal wear on the left wheel occurred relatively slowly. Hence from these observations, comparing both wheels at the beginning of the experiment, it can be concluded that rail surface smoothness directly impacted the wheel polygonization. Since we utilized the Python language script to change the rail surface roughness, the methodology we employed in this study to assess the impact of rail surface roughness on wheel wear forces.

2.2 Finite element model

Finite Element Analysis (FEA) is a widely used numerical method for simulating complex engineering systems. In this case of a wheel set and a rail, FEA is used to model the structural behavior of the system under various loading conditions, such as static, and dynamic loads. The finite element model of a wheel set and a rail consists of dividing the system into small elements and solving the governing equations for each element. The model considers the material properties, geometry, and boundary conditions of the components, such as the wheel, and the rail. The model also accounts for the contact between the wheel and rail and the resulting forces and stresses. The corrugated or waved track is the most common cause of increased roughness in the longitudinal direction during railway operation. The influenced area on the rail is often irregular; its length can range from several tens of millimeters to hundreds of millimeters, and the maximum depth of the groove reaches tens of microns. To analyse forces within the rail finite element model, based on [21], the rail finite element model is assumed to behave as a beam supported by a linear elastic foundation to analyze numerous different forces acting on it. In this study, numerical train run simulations were carried out. The proposed train speed is 30km/hr, for all experiments. Initially as train speeds increase, contact pressure and frictional stresses also increase.

Structural components in high-speed rail systems should be designed to accommodate these high frictional stresses and contact pressures to reduce abrasion and wear on the contact interface surfaces. The finite element model of a wheel set and a rail is an important tool for analysing the structural behavior of the system and improving its design and performance. This technique allows engineers to predict and optimize the behavior of the system under different operating conditions, leading to safer and more efficient rail systems.

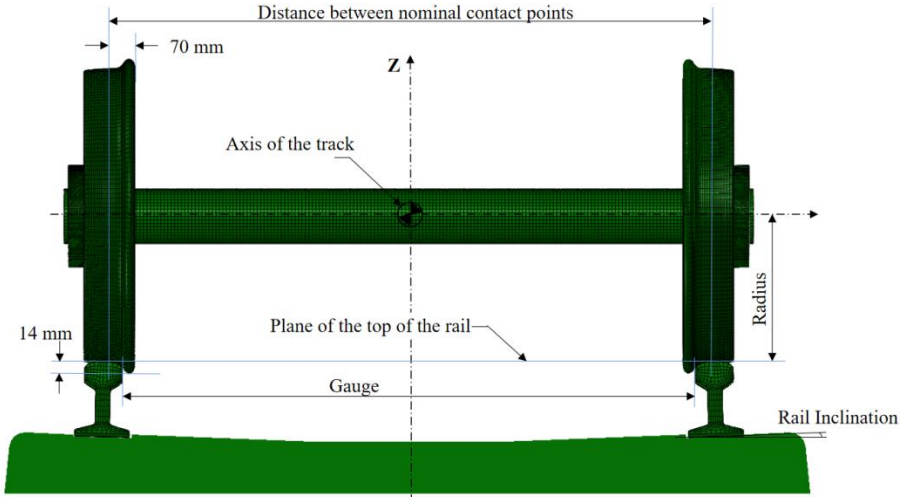

Figure 3. Geometry of the Finite Element model

Hypermesh is used to create all the components; the wheelset, a couple of rails, elastic rubber components for the wheels, which absorb vibration inside the wheels, sleepers, and a slab. The meshed components are then imported into the finite element software ABAQUS for assembly. The finite element model of the system after the components are fully assembled is shown in Figure 3 above. The element types in the model are all non-conforming elements C3D8R with 1,283,552 linear hexahedral elements. The total number of model elements is 1,318,880, the total number of nodes is 1,406,458, and there are 35,328 linear wedge elements of type C3D6. The wheel set-track contact parts are refined by using transition mesh.

In the numerical methods, it should be pointed out that the precision largely depends on the mesh size and the geometric representation used for roughness. The mesh is divided by using a structured and swept technique using Hypermesh. Meanwhile, the nominal rolling diameter of the wheel is d= 0.84m, and the tread type is China's LMA worn-type tread. The length of the axle is as La= 1.966m. The length of the rail is set as Lr= 3m. The average load capacity of rail wheel set is above 908kgs. In this paper, each component of a freight car wheel set weighs 355kgs. And a wheel set is comprised of 1 axle with 2 wheels (bearings are considered negligible here). The wheel set used in this paper is 1065.4kg of weight. Each freight car (usually) has 4 of these. The average mass of the rail is 60kg/m. The distance between the rails is 1582mm, and the bottom slope value of the rail is 1/40. The average dynamic friction coefficient between the wheel and rail is μ = 0.3. The EN standard, the EA1N and EA4T steel grades are widely used for railway axles. In this paper, the main components of our model are the CN standard, the Rail_CN60, and the WJ-8 type of elastic fastening system. The materials of the wheel and axle were the same, homogeneous, and isotropic, with ideal elastic-plastic behavior.

2.3 Study Design

The track geometry condition of the track is usually inspected by light or heavy truck geometry inspection cars twice or three times annually, depending on the rail class. Due to increased axle loads and operational speeds in recent decades, track geometry is deteriorating at a faster rate; as such, there is a need to inspect the track more frequently.

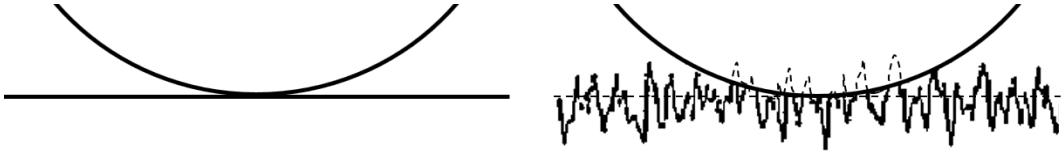

(a) Smooth Rail (b) Rough Rail

Figure 4. Rail surface profiles in contact with the wheel

The inaccuracy of the geometry inspection cars and their operational costs limits the number of frequencies for carrying out this roughness measuring process. This results in the rail system operating with ignored surface roughness for a period. Figure 4 above shows a wheel in contact with a smooth rail surface (4a) and a wheel in contact with a rough rail surface (4b). Figure (4a) is an ideal model because there is always a coefficient of roughness on the surface of the rail. This surface roughness varies depending on the rail system's operational conditions, the rail's material components, and the rail's service life. Using our vehicle-turnout coupling model, after setting the initial wheel profiles and calculation parameters, complete a full wheel-rail contact simulation to confirm the model validity. This model is the default model for our experiment series saved as data set A same as Figure 4(a) smooth rail. To obtain our experimental results for this paper with less experiment time, only the left wheel contact analysis was used for results analyses. Table 1 shows the Data which values which were used to change rail surface roughness in this papers experiments. Y_Wavelength is the difference between the maximum and minimum Y coordinates for Data sets A to H respectively.

$$T_G = 2P/\sigma E^* \sqrt{2B\sigma} \quad \text{and} \quad \mu = \frac{8}{3}\eta\sigma\sqrt{2BR} \tag{3}$$

Where R the radius of the wheel usually denoted by β in the (greenwood's cp formula). Since these are related to variables which would in practice be known.T_G is the non-dimensional parameter of Greenwood method.The effect of μ is small when the wheel is in contact with rougher surfaces. Once the statistical parameters defining each case have been calculated it is possible to calculate the non-dimensional parameters 'T_G' and 'μ' for each roughness profile. To calculate 'T_G' and 'μ', a normal load of 660×10^3N and a radius of 0.46m have been used. The track geometry condition of the track is usually inspected by light or heavy truck geometry inspection cars twice or three times annually, depending on the rail class.

Due to increased axle loads and operational speeds in recent decades, track geometry is deteriorating at a faster rate; as such, there is a need to inspect the track more frequently. The inaccuracy of the geometry inspection cars and their operational costs limit the number of frequencies for carrying out this roughness measuring process. This results in the rail system operating with ignored surface roughness for a period of time. Table *1* shows the Y_Wavelength values, which are the difference between the maximum and minimum Y coordinates for data sets A to H, respectively. Once the statistical parameters defining each case have been calculated, it is possible to calculate the non-dimensional parameters for each roughness profile.

Table 1 Data Set values used to change surface roughness in this paper

Data	Y_Wavelength (mm)	Roughness (mm/RMS)	T_G Value	μ_G / η	Average radius (mm)
SET A	N/A	Ideal smooth	N/A	0.30	N/A
SET B	0.15	1.061E-04	2105	0.18	0.06
SET C	0.35	2.475 E-04	591	0.43	0.18
SET D	0.71	4.950 E-04	209	0.85	0.35
SET E	1.41	9.890 E-04	73.9	1.72	0.17
SET F	2.82	1.979 E-03	26.1	3.43	1.41
SET G	5.66	3.960 E-03	9.2	6.86	2.83
SET H	11	7.920 E-03	3.2	13.71	5.61

In Table 1 above, (x, y, z) roughness coordinates used in this paper's simulations, $T_G$value and Average Radius are values are given. Eight simulations were carried out using the Abaqus Python interface, changing the rail surface roughness with the coordinates below. Data sets A (ideal smooth surface), B, C, D, E, F, G, and H simulation results are compared to determine the impact of rail surface roughness on the wheel wear rate and polygonization. Wootae Jeong [9], in his Acoustic Roughness Measurement of Railhead Surface experiment, in Figure 9 found that the rail surface roughness is within the range -600 and +200 micrometers. This paper used Wootae's observation to derive the surface roughness coordinates.

2.3.1 Verifying the Roughness profile on rails

Verifying the roughness profile on rails is an important part of ensuring that the rails are within the acceptable tolerance levels for safe and efficient train operation. There are several methods for measuring rail roughness, including contact and non-contact methods.

a. Contact methods involve physically touching the rail surface with a probe or stylus to measure the surface profile. These methods can be precise and accurate, but they can also be time-consuming and require specialized equipment. Some common contact methods for measuring rail roughness include the stylus method, the needle probe method, and the ball probe method. Figure 5 below shows how the wheel set contact surface vibrates during contact with rails of different surface roughness between the time intervals of 0.5s and 14s.
b. Non-contact methods do not physically touch the rail surface and instead use various technologies to measure the surface profile. These methods can be faster and less expensive than contact methods, but they may not be as precise or accurate. Some common non-contact methods for measuring rail roughness include laser scanning, optical profilometry, and 3D imaging.

Regardless of the method used, it is important to establish acceptable tolerance levels for rail roughness and to regularly monitor and maintain the rails to ensure they remain within these tolerances. Regular inspections and maintenance of rails can help to ensure safe and efficient train operation, as well as prolong the life of the rails themselves. By verifying the roughness profile on rails and taking appropriate corrective actions, railway operators can minimize the risks associated with rail wear and ensure smooth and reliable train operation.

In this paper, to verify that the python code used to change the roughness of rail surfaces was successful, Figure 5 below shows the left wheel displacement against time graphs for eight data sets. Roughness density (μ) which is the number of peaks per unit area, is difficult to measure in Abaqus, hence, the vibrations of the wheel surface profiles are compared using displacement comparisons.

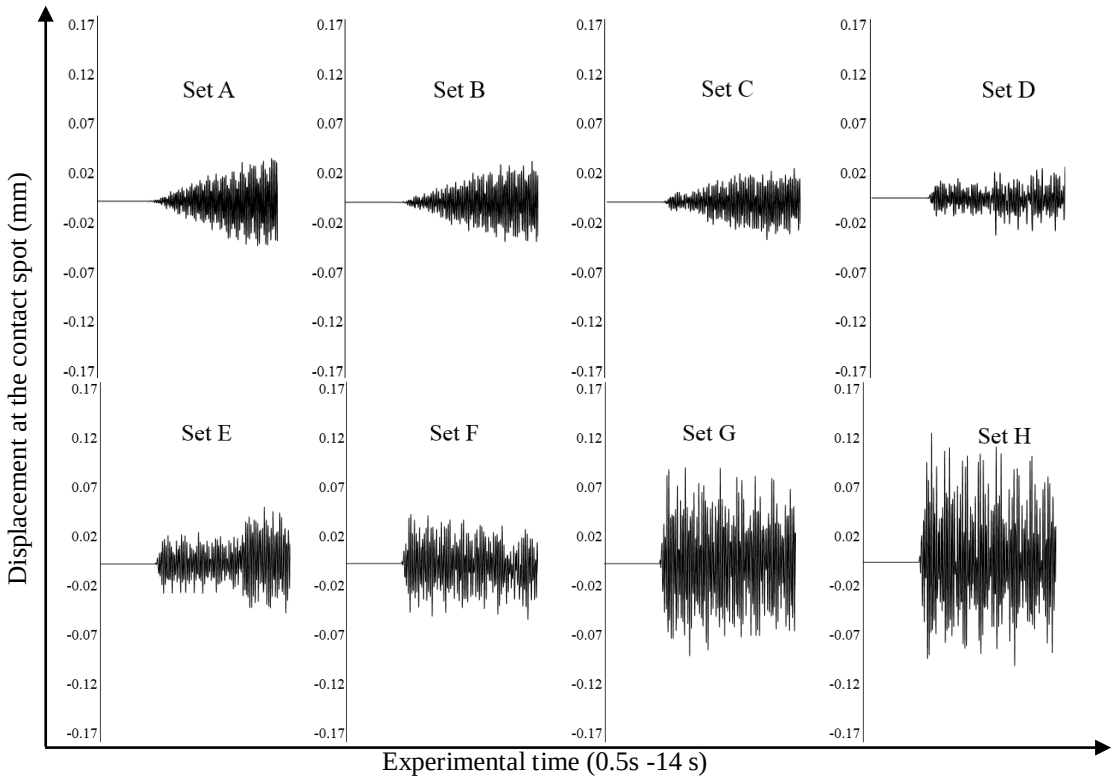

Figure 5. Contact spot displacement at the beginning of the rolling process

In order to adapt to future development and needs, this study prototypes the Chinese high-speed rail transit vehicle and adjusts the wheel parameters of the original rail transit system. In many studies, track irregularities are considered as an important source of car body dynamic excitation, which is elaborated by some scholars [19], [20].

2.3.2 Model Validity

The Hertzian theory of contact pressure was used as a reference to verify the validity of the wheel rail contact in the paper. The theory is a widely accepted method for analysing the stresses and deformations that occur at the contact interface between two elastic bodies. In the context of a wheel-rail contact, the Hertzian theory can be used to predict the stresses and deformations that occur at the contact point between the wheel and the rail. The Hertzian theory assumes that the contact between two elastic bodies is a small, circular area of contact. It further assumes that the two bodies are perfectly smooth and that the contact is under normal force. In the case of a wheel-rail contact, the normal force is provided by the weight of the vehicle.

Using the Hertzian theory, the maximum pressure that occurs at the contact point between the wheel and the rail can be calculated as: $P_{max} = (3F)/(2\pi ab)$, where P_{max} is the maximum pressure, F is the normal force, a and b are the major and minor radii of contact, and π is the mathematical constant pi.

The Hertzian theory can also be used to calculate the contact deformation at the contact point. The deformation can be calculated as: $D = (3F)/(4E\sqrt{a}$, where D is the deformation, and a is the radius of contact.The theory has limitations, such as the assumption that the two bodies are perfectly smooth and that the contact is under a normal force. In reality, the wheel and rail have rough surfaces, and the contact is under a complex combination of normal and tangential forces. Therefore, the Hertzian theory is often used in combination with other contact models to obtain a more accurate representation of the wheel-rail contact. The theory of contact provides a useful method for predicting the stresses and deformations that occur at the contact point between the wheel and the rail. It is a widely accepted theory that provides a good approximation for simple contact cases. However, in complex wheel-rail contacts, the Hertzian theory needs to be used in combination with other contact models to obtain a more accurate representation of the contact.The theoretical value is calculated according to the load conditions and the contact spot area, and the actual value is tested according to the results of the simulation experiment.

3. Analysis of Rail and Wheel Contact Area

In order to express the maximum contact pressure and contact stresses in terms of the applied load, equivalent radius, and extended equivalent modulus, a simple form of the Hertz theory is used. The Hertz hypothesis is invalid when the wheel and rail in contact are coated with other coating materials.

3.1 Normal surface displacement

To analyse contact area forces, consider the frequency response function (FRF) of the normal surface displacement due to pressure on a 3D body's surface as:

$$\overline{\overline{u}} = \frac{1-\nu_c}{\mu_c w} \cdot \frac{1+4wh\varsigma\beta - \lambda\varsigma\beta^2}{1-\left(\lambda+\varsigma+4\varsigma w^2h^2\right)\beta+\lambda\varsigma\beta^2} \tag{4}$$

Where

$$\lambda = 1-\frac{4\left(1-\nu_c\right)}{1+\mu\left(3-4\nu_s\right)},\ \varsigma = \frac{\mu-1}{\mu+\left(3-4\nu_c\right)},\ \beta = \exp\left(-2wh\right),\ \mu=\mu_c\ /\ \mu_s$$

μ is the shear modulus, ν_i is the Poisson ratio, subscripts 1 and 2 refer to bodies wheel and rail as shown in Figure 6 below, subscripts *c* and *s* refers to coating and substrate, *h* is the coating thickness, λ and ς are constants similar to Dundurus parameters. The double tilde means two-dimensional Fourier transform with respect to (*x*, *y* and *w*) is defined in the frequency domain and is the counterpart of radius in the space domain.

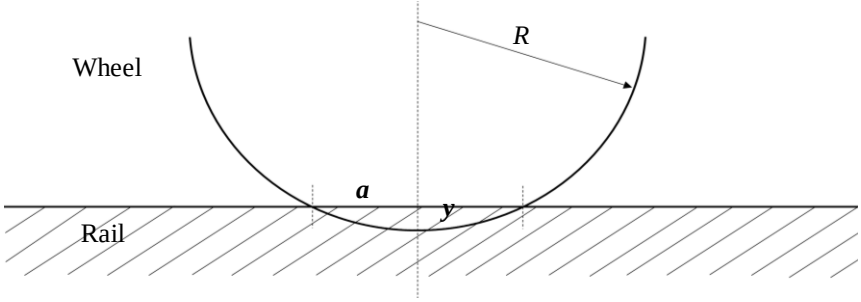

Figure 6**.** Wheel-rail micro contact and the Hertzian Classical contact theory

The Hertzian analysis cannot hold for rough surfaces. Even if the asperities in the central area are so deformed as to create a region of essentially continuous contact, this will be surrounded by a fringe in which only the higher asperities touch [22]. Further from the center the gap between the surfaces widens and there will be fewer asperities which bridge it. Thus, instead of the continuous contact and the resulting continuous pressure distribution envisaged in the Hertzian analysis we must consider the force between rough solids to be the sum of a set of individual forces transmitted through an array of discrete contact spots. Over each small area of the surface the collective effect of these individual forces can be treated statistically as a pressure. Higher pressures may correspond to a higher density of contact spots or to larger individual spots.

The 2D FRF for body 1 simply is the 3D FRF with w replaced by ω, the counterpart of x, where $\beta = \exp(-2\omega h)$ and the tilde means one-dimensional Fourier transform with respect to *x*. The rough surface limiting situation can be obtained using the assumption that our rail and wheel in contact have no coating (h=0, β=1).

$$\bar{u} = \frac{1-\nu_c}{\mu_c \omega} \cdot \frac{1-\lambda\varsigma}{1-(\lambda+\varsigma)+\lambda\varsigma} = \frac{1-\nu_s}{\mu_s \omega} \tag{5}$$

Using the identity,

$$\frac{1-\lambda\kappa}{1-(\lambda+\kappa)+\lambda\kappa} = \frac{E_c^*}{E_s^*},\ E_i^* = \frac{E_i}{1-\nu_i^2} = \frac{2\mu_i}{1-\nu_i}$$

Where E_i^* with $i = c$ or s is the equivalent modulus. Since the rail and the wheel both have no coatings, the mechanical responses of the rail model are due to the contribution of the substrate materials. The mechanical problems of the rail and wheel are due to the surfaces' smoothness and materials substrate. Hence rewrite the equation (5) with equivalent modulus instead of shear modulus.

$$\bar{u} = \frac{2}{E_s^*}\frac{1}{\omega} \tag{6}$$

Assuming that at the point of contact, both rail and wheel have a curvature since the steel material used in both rail and wheel is elastic. For contact between the wheel and rail, the equivalent Young's modulus becomes:

$$\frac{1}{E^*} = \left[\frac{1-\nu_1^2}{E_1} + \frac{1-\nu_2^2}{E_2}\right] \tag{7}$$

Where E^* the combined elasticity is related to the Young's modulus, E_1, E_2 are the Young Modulus for the wheel and rail respectively. The Hertzian analysis for the contact between the wheel of radius R and rail beam can be expressed in terms the distance y which points away from the deformation zone move together during the deformation in Figure 6 above. The area of contact A_1 and the load P_1 are then expressed as below:

$$A_i = \pi R s\ , \qquad P_i = \frac{4}{3} \times E^* R^{1/2} s^{3/2} \tag{8}$$

If the separation of the rail and wheel nominal surfaces at the position of maximum contact is u, there will be contact at that asperity if its height z is greater than u. The probability of this is:

$$\text{prob}\ (z > u) = \int_u^\infty \phi(z) dz \tag{9}$$

Where $\phi(z)$ is the probability density function of the distribution of contact (peak) heights. Also, assuming that the contact occurs first at the highest point (which is true if the slope of the surface is not too large), the compliance *s*will be equal to $z-u$, and the resulting contact area A_i will be $\pi R(z-u)$. Hence the contact area and the expected force at this same contact, is expressed as:

$$\overline{A_i} = \int_u^\infty \pi R(z-u)\theta(z)dz\ , \qquad \overline{P_i} = \int_u^\infty \frac{4}{8} E^* R^{\frac{1}{2}} (z-u)^{\frac{3}{2}} \theta(z)dz \tag{10}$$

Let η be the density of asperities, and consider an element of surface da over which the separation between the nominal surfaces is *u*.

Then the expected number of contacts dN , the expected real are of contact dA , and the expected load occurring within dP will be:

$$dN = \eta da \int_{u}^{\infty} \phi(z)dz \tag{11}$$

$$dA = \pi\eta\beta da \int_{u}^{\infty} (z-u)\phi(z)dz \tag{12}$$

$$dP = \frac{4}{3}\eta E^{*}\beta^{1/2} da \int_{u}^{\infty} (z-u)^{3/2}\phi(z)dz \tag{13}$$

Hence taking the force dP on the area da to be equivalent to uniform pressure p , the pressure distribution is given by $p = \lambda F_{3/2}(u/\sigma)$. $F_{3/2}(u/\sigma)$ values are obtained using numerical integration[23]. σ is standardised variable that describe the heights of asperities in terms of the standard deviation a of the height distribution. Sigma is the surface roughness, since it is a measure of the same kind as the technological measures of roughness such as the center line average (CLA). The analysis process of a rigid wheel-rail coupling system is divided into two steps: static pressure and rolling. Since the wheel-rail contact theory is only applicable to static or quasi-static conditions, with the increase in wheel rolling speed, the wheel-rail system gradually does not meet the calculation conditions of the wheel-rail contact theory, so the theoretical value of the maximum contact pressure is calculated before the rolling of the wheel. Table 2 and Table 3 below shows a sectional view of the wheel and rail interaction at the beginning of the static loading process for data sets A to H.

Table 2 Data Set A-D, wheel-rail contact stress (t=0.05s)

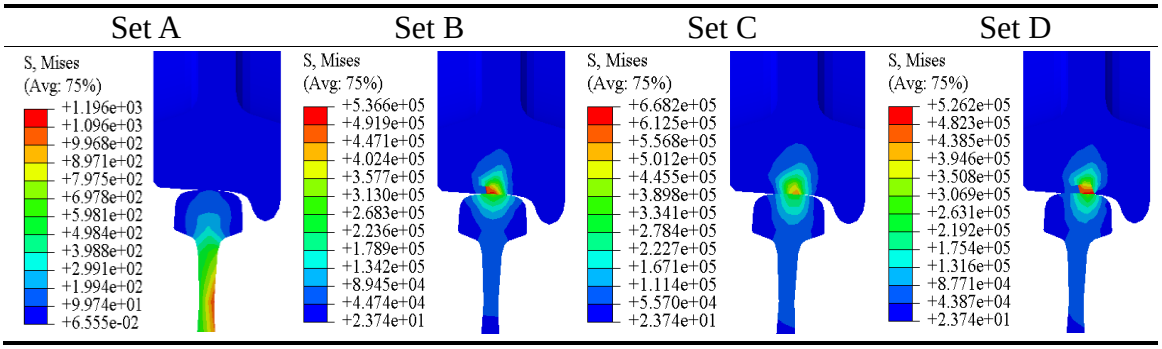

As shown from the Table 2 above, data set A has the lowest contact stress value, 1.196×10^{-3} MPa. The contact stresses in set A are more concentrated in the middle section of the rail beam. Set B, C, and D contact stresses are more concentrated at the wheel rail contact spot.

Table 3 Data Set E-H, wheel-rail contact stress (t=0.05s)

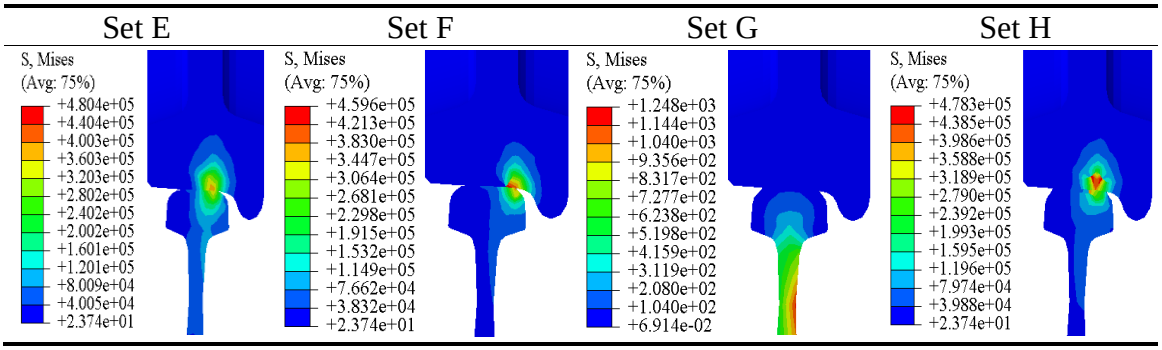

Table 3 above shows a sectional view of the wheel and rail at the beginning of the static loading process at time t= 0.05s for data sets E-H. As shown from the table, data set H has the greatest value of contact stress, 0.478MPa. The contact stresses in set E, F, and H are not concentrated in the middle of the contact area as compared to those in Table 2.

In Table 3, the contact stresses are more aligned closer to the rail edge. The contact stresses in set G are more concentrated in the middle section of the rail beam. From the Table 2 and Table 3 above, it can be seen that the contact stresses deviate from a standard pattern. There is an increase in maximum contact stress from 1.196×10^{-3} MPa (set A) to a value of 0.668 MPa (set C). The maximum contact stress then constantly decreases from set C to a value of 0.478 MPa (set H). It is a widely accepted theory that provides a good approximation for simple contact cases. However, in complex wheel-rail contacts, the Hertzian theory needs to be used in combination with other contact models to obtain a more accurate representation of the contact.

Since the wheel-rail contact theory is only applicable to static or quasi-static conditions, another analysis is done in Table 4 and Table 5 below, at the moment just before the train takes off. After 0.26s, at the end of the loading process, the average contact stresses increased by a big margin as compared to the tables at the beginning of the loading process.

Table 4 Data Set A-D, wheel-rail contact stress (t=0.26s)

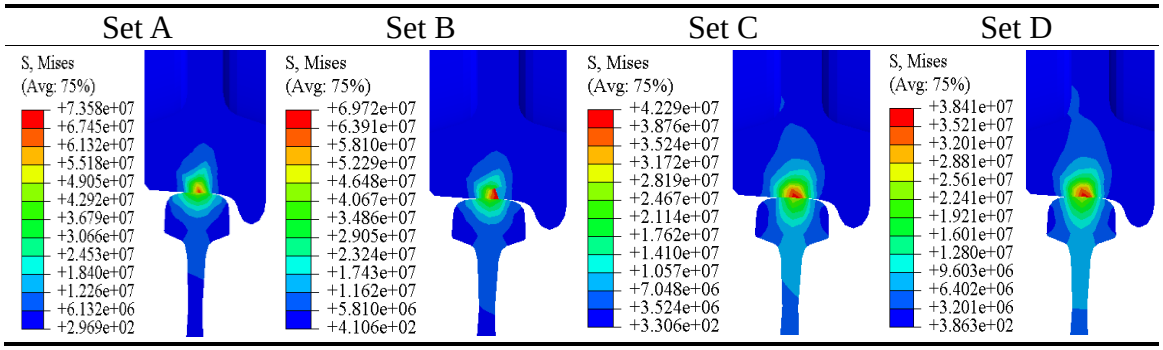

Table 4 above shows there is a constant decrease of maximum contact stress from set A to set D. Set A has the maximum contact stress of 73.58 MPa. The contact stresses are more concentrated at the middle of the contact spot for all sets.

Table 5 Data Set E-H, wheel-rail contact stress (t=0.26s)

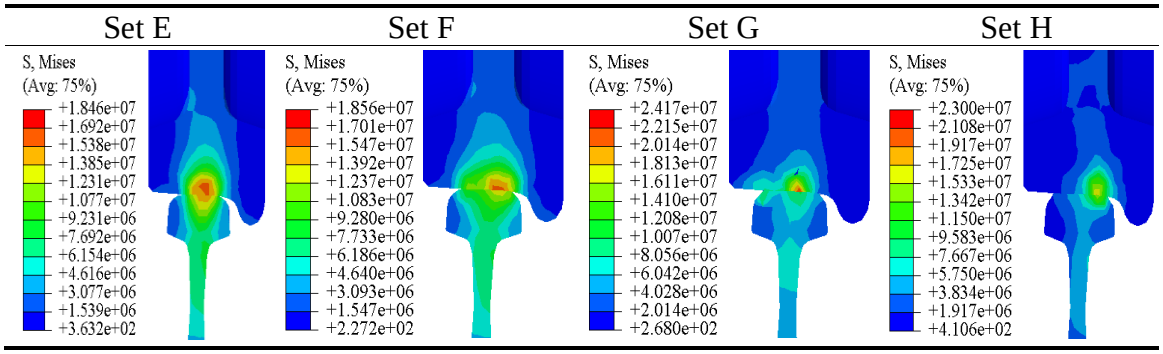

From Table 5 above, there is a constant increase in maximum contact stresses from 18.46MPa (set E) to a value of 24.17MPa (set G). Set E and Set F show that there are more than average stresses spreading into the rail's vertical profile. As the surface roughness increases, the contact stresses spread more.

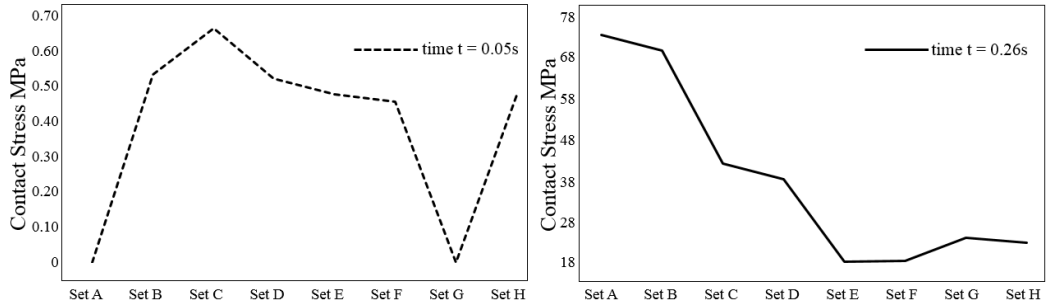

Figure 7. Wheel-rail maximum contact stress distribution

Figure 7 above shows the maximum contact stress distribution for the wheel-rail contact as the rail surface roughness increase at the initial and final stages of the static loading processes respectively. The stress cloud diagrams show the rigid wheels in contact with rails of different surface roughness. The wheel-rail coupling system is analysed at time t = 0.05s and t = 0.26s, respectively, under static loading pressure. During the static contact process, the maximum contact stress of all rigid wheels in contact with smoother rails is located at the wheel-rail contact position. The maximum stress forces are concentrated at the centroid of the rail's contact area. At the beginning of the static loading process, the maximum stress forces of the wheel rail contact are significantly small and are more concentrated outside the wheel contact area. There is a significant increase in maximum contact stress as roughness increases from Set A to Set B. At the end of the static contact process, the maximum contact stresses decrease uniformly with the increase in roughness. As the surface roughness increases, the depth of stress increases along the vertical direction of the rail.

3.2 Contact Area with Rail Surface Roughness

The wheel-rail contact area is a critical factor in determining the wear rate of wheels and rails in railway systems. One of the key factors influencing the contact area is the surface roughness of the rail. Our results show that as rail surface roughness increases, the contact shape between the wheel and rail changes, leading to an increase in contact pressure and a reduction in contact area. These changes in contact shape and pressure distribution can lead to increased wheel wear, which is consistent with previous studies. As rail surface roughness increases, the contact area between the wheel and rail decreases. This reduction in contact area can lead to increased wear on both the wheel and rail[24], [25]. Figure 8 below shows the contact area against the distance travelled by the wheel between the distances of 1500mm and 2000mm.

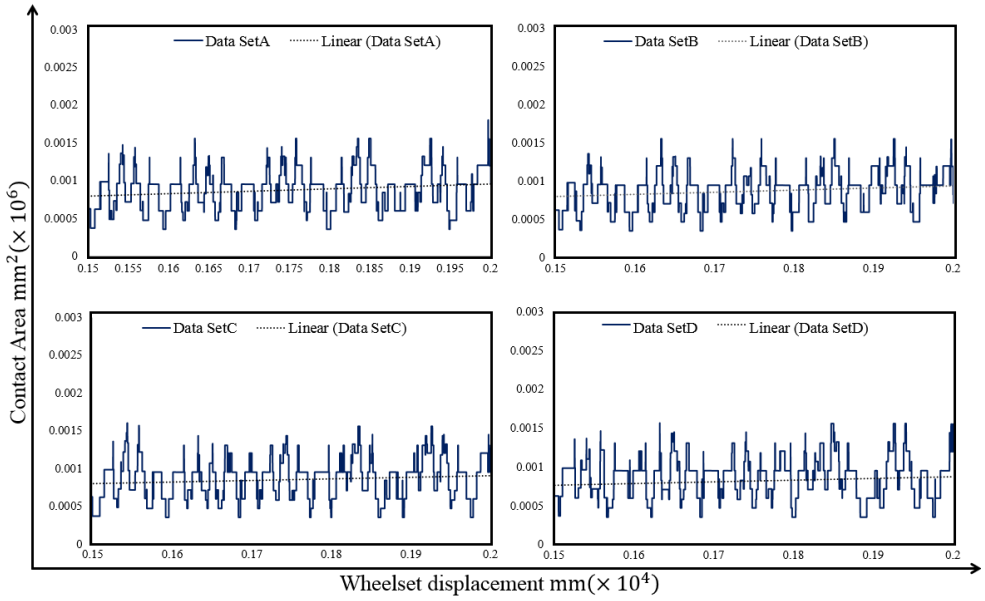

Figure 8. Contact area between distances 1500mm and 2000mm (Sets A to D)

As shown by the microscopic contacts in the graphs, sets A to D shows that there is always a contact above $300mm^2$ throughout the journey. The linear trend line gradients for sets A, B, C, and D are 0.32, 0.28, 0.21 and 0.22 respectively. Data set A has the steepest slope and the maximum contact area value of $1803.4mm^2$. Data set C has the minimum contact area of value $345.3mm^2$ .Figure 9 below shows the contact area during the rolling process between the distances of 1500mm and 2000mm for data set E-H.

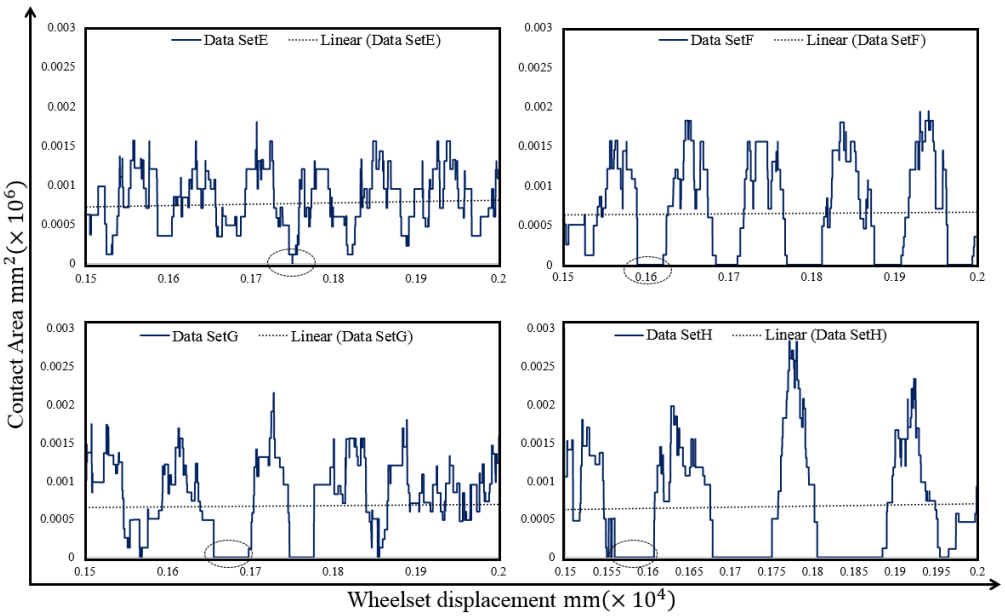

Figure 9. Contact area between the distances 1500mm and 2000mm (Sets E to H)

As shown in Figure 9 above, the graphs for data sets E to H are more spaced as compared to those of sets A to D. For data Set D, the contact area slightly touches the $0mm^2$ axis between the distance of 1700mm and 1800mm. Set F,G, and H, shows a greater distance at which the contact area is approximately equal to $0mm^2$. The microscopic contact graphs show that data set H has a greater distance travelled in which the contact area is approximately $0mm^2$. The wheel in contact with the roughest surface set H has the maximum contact area value of $2835.5mm^2$ as shown in the figure. From the linear trend lines, it can be observed that set E has the maximum gradient of a value 0.175 and set F has the minimum gradient, which is equal to 0.065.

3.3 Maximum contact area

The maximum contact area between the wheel and rail is affected by rail surface roughness. Typically, as rail surface roughness increases, the average contact area between the wheel and rail decreases due to the reduction in the effective contact length. Several studies have investigated the relationship between rail surface roughness and maximum contact area. For example, a study found that the maximum contact area decreased as the rail surface roughness increased [26], [27]. Similarly, it was observed that an increase in rail surface roughness resulted in a reduction of the maximum contact area.

However, it is worth noting that the specific relationship between rail surface roughness and maximum contact area can depend on various factors, such as the wheel and rail material properties, applied loads, and contact conditions. Therefore, a comprehensive investigation of these factors is needed to fully understand the effect of rail surface roughness on the maximum contact area between the wheel and rail. The results of this paper stipulate that as surface roughness increases, the maximum contact area between the wheel and the rail increases. But it is worth noting that the average contact area decreases at the same time. This is because for wheels in contact with rails on smoother surfaces, there is always contact between the wheel and the rail, whereas with rougher surfaces, the wheel and rail separate several times along the journey. Figure 10 below shows the maximum rail-wheel contact area as the rail surface roughness increases. As shown in the Figure 10, data set H has the largest maximum contact area of value $3208mm^2$ whilst data Set B has the smallest maximum contact area value of $1559mm^2$.

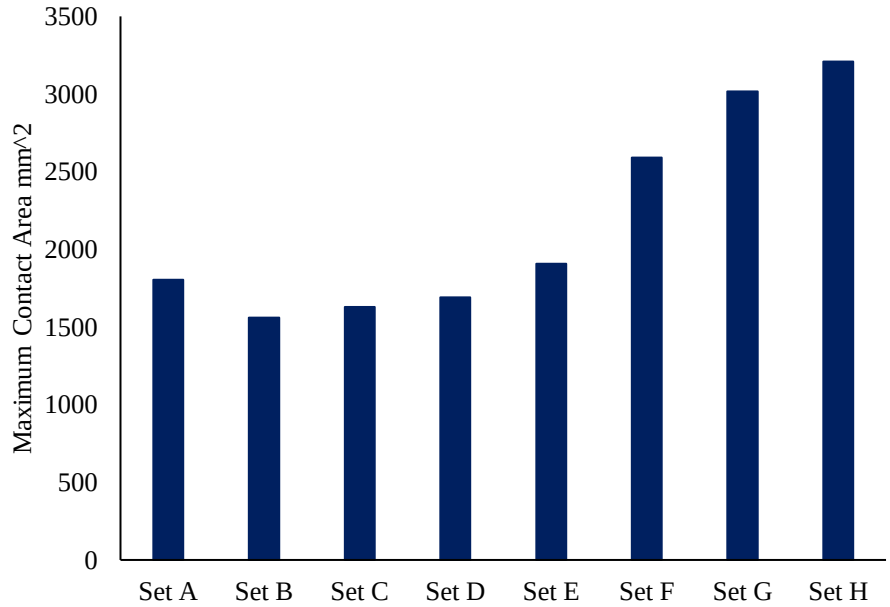

Figure 10. Distribution of Maximum Contact Area with increasing Surface Roughness

The graph shows that initially, as the surface roughness is induced, there is a small drop in the maximum contact area value from set A to set B. From set B to set H, as surface roughness increases, the maximum contact area increases continuously. In conclusion, the maximum contact area of a wheel in contact with a smooth rail surface is larger than the area of the wheel in contact with the rail surface with the smallest roughness coefficient. As the rail surface roughness increases, the maximum contact area between the wheel and the rail also increases.

4. Wear contact Forces

The wear contact forces between the rail and wheel play a crucial role in determining the extent of wear on the wheel. In this section, we will analyse and discuss the wear contact forces in the rail-wheel simulation results obtained for our study on the effect of rail surface roughness on wheel wear. Our analysis will focus on understanding the relationship between the wear contact forces and the different parameters that affect them. We will use the simulation results to quantify the magnitude and distribution of the contact forces and investigate how they vary with changes in the rail surface roughness. By doing so, we aim to provide a comprehensive understanding of the wear contact forces and their underlying mechanisms, which will help us better understand the wear behavior of the rail and wheel system.

4.1 Tangential contact forces

The tangential problem is a critical aspect of understanding the effect of rail surface roughness on wheel wear. The tangential problem refers to the interaction between the contacting surfaces of the rail and wheel, which results in tangential forces that can cause wear on the wheel. The solution to this problem involves understanding the contact mechanics between the two surfaces and determining the resulting frictional forces. Traditionally, the tangential problem has been solved using analytical or numerical methods. Numerous studies have investigated the tangential contact problem for wheel-rail contact, including experimental, analytical, and numerical methods[27]. In this section, the solution of the tangential problem using the numerical method of finite element analysis is discussed. By doing so, we aim to provide a comprehensive understanding of the tangential problem and its role in determining wheel wear, which will contribute to our overall understanding of the effect of rail surface roughness on wheel wear.

Figure 11 below shows the normal contact forces for data sets A, B, C, and D during the static and rolling processes. As shown in the figure, during the wheel loading phase, the tangential contact force between the wheel and the rail increases with a very small margin for all the wheels. For data Set A, the tangential force constantly increases from 0 N at t = 2.28 s to 310N at t = 4.55 s and then drops instantly to 260 N. Whereas for data set C, the graphs show that the force increases constantly with experiment time, from 0 N at the t = 0 s to 240 N at t = 4.10 s, and then sharply increases to a value of 280 N at time t = 4.55 s. For data set D, the tangential force increases more smoothly with time starting from 0 N at t = 0.91 s, to a value of 250 N at a t = 4.55 s.

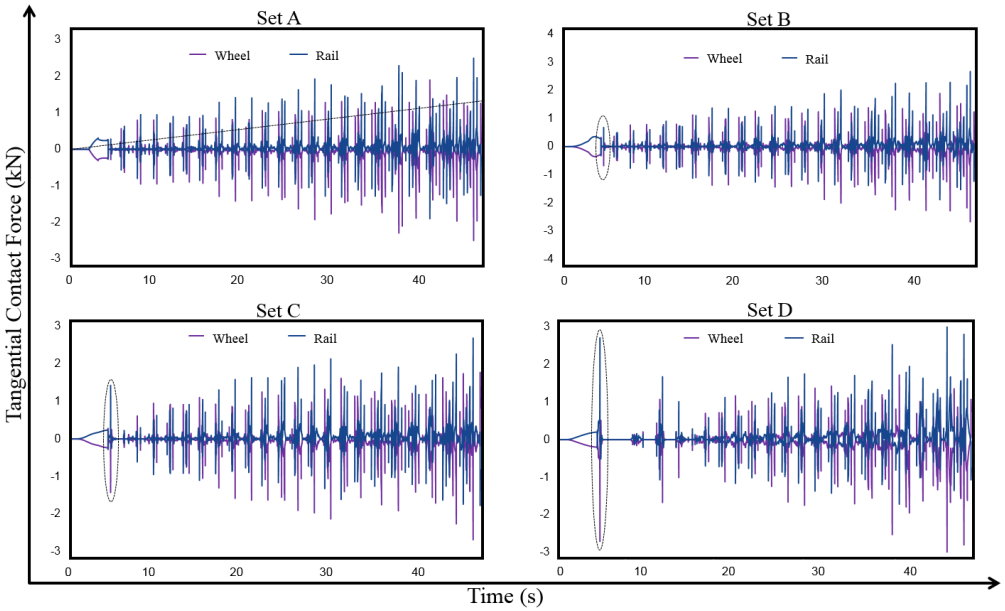

Figure 11. Wheel Rail tangential force (Sets A to D)

During the motion of the wheel, for set A, using the linear trending line, it shows that tangential forces increase gradually with time. For data sets B, C, and D, just after static loading, the tangential force sharply increased, with set D having the maximum value of 2.71kN. The rolling tangential force for set D does not increase uniformly as compared to sets A, B and C.

Figure 12 below shows the wheel-rail tangential contact forces for data sets E to H during the experiment. As compared to the wheels in contact with smoother rail surfaces, data sets E, F, G, and H show random decreases and increases in contact forces throughout the experiment. During the static loading, Data sets E and F show a smooth increase of the contact force with a small gradient as compared to the sets in Figure 12 sets G and H barely show any increase in contact force until the end of the loading process.

During the rolling process, Figure 12 displays that all sets have random increases and decreases of contact forces along the rail path. There is a sharp increase in contact forces right at the beginning of the rolling process for all sets. Set H shows the largest value of maximum contact force, of a value of 48.3kN at the beginning of the rolling process. As compared to set A with a wheel in contact with a smooth rail surface, data sets E, F, G, and H of wheels in contact with rough rail surfaces does not have a standard increase of contact force with time.

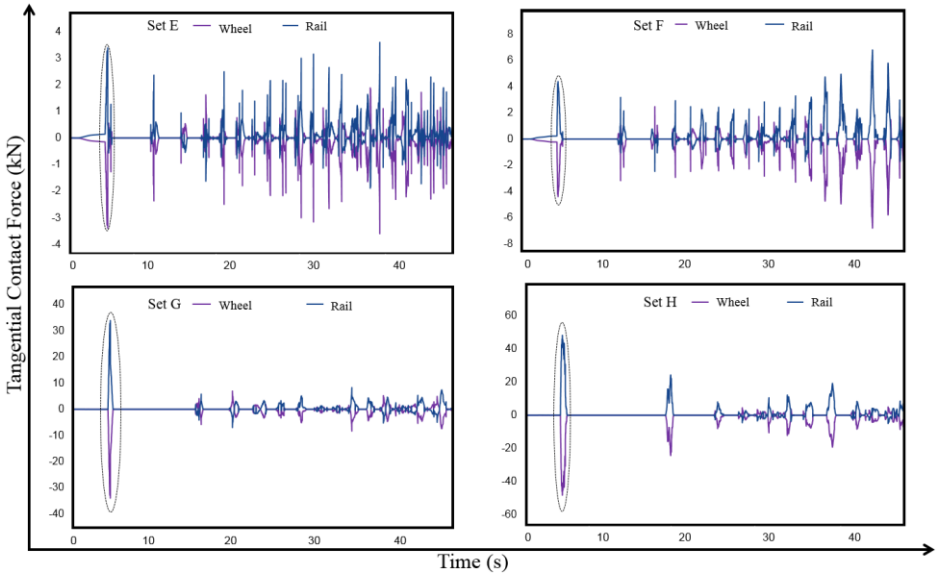

Figure 12. Wheel Rail tangential force (Sets E to H)

4.2 Wear contact forces in comparison with Archard's model

The wear calculation of the wheel-rail system is very complex, and it needs to determine the appropriate wear model. At present, the typical wear models are Archard's model, Pearce's model, USFD's model, Braghin's model, and other models, which are suitable for different scenarios and test conditions, and the wear coefficient K is different. As one of the most classic wear models, Archard's model is suitable for wheel-rail wear calculation. Archard's wear model is widely used in the context of wheel-rail contact analysis to predict the wear of the wheel and rail materials over time[28], [29].

Using Archard's wear model in the wheel-rail contact analysis done with Abaqus has many benefits. First, it is simple to implement and does not require complex numerical simulations. Second, it provides an accurate estimate of the wear rate, which is crucial for determining the maintenance schedule and overall operational costs. Third, it can help in identifying the critical locations of wear, which can help in designing better materials and improving the overall performance of the railway system. The use of Archard's wear model in the wheel-rail contact analysis done with Abaqus is essential for accurate and effective prediction of wear and tear in the railway system. The simplicity and accuracy of the model make it an ideal choice for predicting the wear of the wheel and rail materials over time.

Archard's wear model is one such model that has been extensively used in the past few decades due to its simplicity and effectiveness. Archard's wear model provides a quantitative relationship between the wear volume, the contact force, and the sliding distance. The model is based on the following equation:

$$\frac{V_A}{V_v} = k_A \cdot \frac{N_A}{H_A} \tag{14}$$

Where V_A is the wear volume at the contact position; $V_v = \sqrt{V_\xi + V_\eta}$ is the total slip distance of the wheel, ξ, η is horizontal and vertical respectively; k_A indicating wear coefficient, indicates the probability of obtaining an abrasive particle; N_A is the Normal wheel-rail force; H_A indicates the Vickers hardness of the softer material at contact. ; $F_v = \sqrt{F_\xi + F_\eta}$ is the total tangential force of the wheel and rail; D represents the wheel diameter; the wheel slip speed $\dot{v}_v$ and total tangential force F_v are related to the vehicle speed v_c and normal wheel-rail force N_A and can be expressed as $F_v \cdot \dot{v}_v = k_v \cdot N_A \cdot v_c$, where k_v is the slip coefficient.

The volume wear rate is expressed as follows:

$$\dot{V}_A = k_A \cdot \frac{N_A}{H_A} \cdot \dot{v}_v = k_A \cdot k_v \frac{N_A}{H_A} \cdot v_c \tag{15}$$

Where the contact area between the wheel and the track is A, the wear speed is $\dot{Z}_A$.

$$\dot{Z}_A = \frac{V_A}{A} = \frac{k_A \cdot k_v}{H_A \cdot A} \cdot N_A v_c = \frac{k_A \cdot k_v}{H_A A} \cdot F_v v_c \tag{16}$$

Introduce a coefficient K and define it as

$$K_A = \frac{k_A \cdot k_v \cdot v_c}{H_A \cdot A} \tag{17}$$

Hence wear can be expressed as

$$\dot{Z}_A = K_A \cdot N_A \tag{18}$$

In summary, this model assumes that wear is proportional to the contact force (F), the sliding distance (S), and the hardness of the materials (H). The increase in rail surface roughness causes an increase in contact forces and contact stresses between the wheel and rail, which in turn leads to an increase in wear volume. Figure 13 below shows the maximum contact forces experienced as the surface roughness increases.

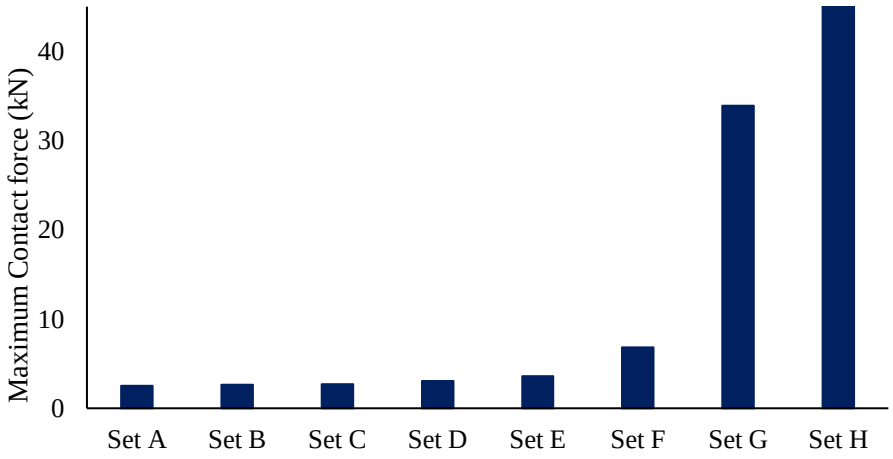

Figure 13. Wheel-rail maximum contact wear force

As shown by the graph, there is a constant small increase in contact forces from data set A to F. The contact force value increases with a huge margin in data set G. Data set H has the highest value of maximum contact force, 48.3kN in contrast to Set A, which has smallest maximum contact force value of 2.5kN. Contact force (F) is an important factor in the Archard wear model because it represents the amount of pressure exerted on the material surfaces in contact. The greater the contact force, the higher the pressure, and the greater the likelihood of wear occurring. In other words, when two surfaces are in contact and subjected to a high contact force, the resulting frictional forces and stresses can cause material removal and wear. Therefore, understanding the relationship between contact force and wear is critical in predicting the lifespan and durability of materials under different loading conditions. Additionally, the Archard wear model assumes that wear is directly proportional to the product of contact force and sliding distance ($F*S$). Therefore, accurate measurement and control of contact force is essential for accurately predicting the wear behavior of materials. Based on the experimental results and Archard's wear model, it can be concluded that the surface roughness of the rail has a significant effect on wheel wear.

5. Conclusion

In conclusion, the findings of this study suggest that surface roughness plays a significant role in the wear of wheels in rail transportation. The simulation results demonstrate a clear correlation between the increase in rail surface roughness, wheel-rail wear contact forces, and contact stresses, which consequently lead to an increase in wear volume. This is because the increased roughness of the rail surface creates more contact points between the wheel and rail, increasing the overall area of contact, and hence the contact forces and contact stresses. As a result, more material is removed from the wheel and rail surfaces due to the increased wear volume.

Therefore, the results of this experiment demonstrate the importance of maintaining a smooth rail surface in reducing wheel wear and prolonging the lifespan of rail transportation systems.It is crucial to take surface roughness into account when doing various experiments to analyse the wheel-rail contact problem. Engineers and maintenance personnel should consider measures to reduce surface roughness, such as grinding or polishing, to mitigate wear and prolong the service life of wheels and rails. Further research can explore the effect of other factors on wheel wear, such as wheel-rail material properties and environmental conditions, to provide a more comprehensive understanding of the wear mechanism in rail transportation.

Acknowledgements

The author(s) disclosed receipt of the following financial support for the research, authorship, and/or publication of this article: This work was partly supported by the National Science Foundation of China (No.11302159), the Principal Foundation of Xi'an Technological University (No.XGPY200213).

References

[1] W. Zhai, X. Jin, Z. Wen, and X. Zhao, "Wear Problems of High-Speed Wheel/Rail Systems: Observations, Causes, and Countermeasures in China," *Appl. Mech. Rev.*, vol. 72, no. 6, pp. 1–23, 2020, doi: 10.1115/1.4048897.

[2] H. Dekker, "Vibrational resonances of nonrigid vehicles: Polygonization and ripple patterns," *Appl. Math. Model.*, vol. 33, no. 3, pp. 1349–1355, 2009, doi: 10.1016/j.apm.2008.01.025.

[3] C. Andersson and A. Johansson, "Prediction of rail corrugation generated by three-dimensional wheel-rail interaction," *Wear*, vol. 257, no. 3–4, pp. 423–434, 2004, doi: 10.1016/j.wear.2004.01.006.

[4] A. No and D. Iitb, "Enlargement of Out-of-Round Wheel," vol. 227, pp. 965–978, 1999.

[5] A. Johansson, "Out-of-round railway wheels-assessment of wheel tread irregularities in train traffic," *J. Sound Vib.*, vol. 293, no. 3–5, pp. 795–806, 2006, doi: 10.1016/j.jsv.2005.08.048.

[6] E. Brommundt, "A simple mechanism for the polygonalization of railway wheels by wear," *Mech. Res. Commun.*, vol. 24, no. 4, pp. 435–442, 1997, doi: 10.1016/s0093-6413(97)00047-5.

[7] P. Meinke and S. Meinke, "Polygonalization of wheel treads caused by static and dynamic imbalances," *J. Sound Vib.*, vol. 227, no. 5, pp. 979–986, 1999, doi: 10.1006/jsvi.1999.2590.

[8] X. Jin, L. Wu, J. Fang, S. Zhong, and L. Ling, "An investigation into the mechanism of the polygonal wear of metro train wheels and its effect on the dynamic behaviour of a wheel/rail system," *Veh. Syst. Dyn.*, vol. 50, no. 12, pp. 1817–1834, 2012, doi: 10.1080/00423114.2012.695022.

[9] W. Jeong and D. Jeong, "Acoustic roughness measurement of railhead surface using an optimal sensor batch algorithm," *Appl. Sci.*, vol. 10, no. 6, pp. 1–11, 2020, doi: 10.3390/app10062110.

[10] D. Jeong, H. S. Choi, Y. J. Choi, and W. Jeong, "Measuring acoustic roughness of a longitudinal railhead profile using a multi-sensor integration technique," *Sensors (Switzerland)*, vol. 19, no. 7, pp. 1–18, 2019, doi: 10.3390/s19071610.

[11] E. Verheijen, "A survey on roughness measurements," *J. Sound Vib.*, vol. 293, no. 3–5, pp. 784–794, 2006, doi: 10.1016/j.jsv.2005.08.047.

[12] S. L. Grassie, "Rail corrugation: Advances in measurement, understanding and treatment," *Wear*, vol. 258, no. 7–8, pp. 1224–1234, 2005, doi: 10.1016/j.wear.2004.03.066.

[13] P. Haji Abdulrazagh, M. T. Hendry, M. Gül, A. Roghani, and E. Toma, "Use of measured accelerations from a passenger rail car to evaluate ride quality and track roughness – A case study," *Proc. Inst. Mech. Eng. Part F J. Rail Rapid Transit*, vol. 236, no. 6, pp. 733–742, 2022, doi: 10.1177/09544097211041459.

[14] F. Mauz, R. Wigger, T. Wahl, M. Kuffa, and K. Wegener, "Acoustic Roughness Measurement of Railway Tracks: Implementation of a Chord-Based Optical Measurement System on a Train," *Appl. Sci.*, vol. 12, no. 23, 2022, doi: 10.3390/app122311988.

[15] O. E. Lundberg, A. Nordborg, and I. Lopez Arteaga, "The influence of surface roughness on the contact stiffness and the contact filter effect in nonlinear wheel-track interaction," *J. Sound Vib.*, vol. 366, pp. 429–446, 2016, doi: 10.1016/j.jsv.2015.12.026.

[16] H. Chen, A. Namura, M. Ishida, and T. Nakahara, "Influence of axle load on wheel/rail adhesion under wet conditions in consideration of running speed and surface roughness," *Wear*, vol. 366–367, pp. 303–309, 2016, doi: 10.1016/j.wear.2016.05.012.

[17] R. Lewis, P. Christoforou, W. J. Wang, A. Beagles, M. Burstow, and S. R. Lewis, "Investigation of the influence of rail hardness on the wear of rail and wheel materials under dry conditions (ICRI wear mapping project)," *Wear*, vol. 430–431, no. January, pp. 383–392, 2019, doi: 10.1016/j.wear.2019.05.030.

[18] J. F. Aceituno, P. Wang, L. Wang, and A. A. Shabana, "Influence of rail flexibility in a wheel/rail wear prediction model," *Proc. Inst. Mech. Eng. Part F J. Rail Rapid Transit*, vol. 231, no. 1, pp. 57–74, 2017, doi: 10.1177/0954409715618426.

[19] R. Luo, B. Liu, and S. Qu, "A fast simulation algorithm for the wheel profile wear of high-speed trains considering stochastic parameters," *Wear*, vol. 480–481, no. April, p. 203942, 2021, doi: 10.1016/j.wear.2021.203942.

[20] Y. Wu *et al.*, "Polygonal wear mechanism of high-speed wheels based on full-size wheel-rail roller test rig," *Wear*, vol. 494–495, no. January, p. 204234, 2022, doi: 10.1016/j.wear.2021.204234.

[21] U. Zerbst, R. Lundén, K. O. Edel, and R. A. Smith, "Introduction to the damage tolerance behaviour of railway rails - a review," *Eng. Fract. Mech.*, vol. 76, no. 17, pp. 2563–2601, 2009, doi: 10.1016/j.engfracmech.2009.09.003.

[22] J. A. Greenwood and J. H. Tripp, "The elastic contact of rough spheres," *J. Appl. Mech. Trans. ASME*, vol. 34, no. 1, pp. 153–159, 1964, doi: 10.1115/1.3607616.

[23] J. A. Greenwood and J. B. P. Williamson, "Contact of nominally flat surfaces," *Proc. R. Soc. London.*

Ser. A. Math. Phys. Sci., vol. 295, no. 1442, pp. 300–319, 1966, doi: 10.1098/rspa.1966.0242.

[24] H. F. Kashani and J. P. Hyslip, "Ballast life and effective parameters," *2018 Jt. Rail Conf. JRC 2018*, no. Stage C, pp. 6–9, 2018, doi: 10.1115/JRC2018-6106.

[25] W. J. Wang, H. F. Zhang, Q. Y. Liu, M. H. Zhu, and X. S. Jin, "Investigation on adhesion characteristic of wheel/rail under the magnetic field condition," *Proc. Inst. Mech. Eng. Part J J. Eng. Tribol.*, vol. 230, no. 5, pp. 611–617, 2016, doi: 10.1177/1350650115606480.

[26] Y. Zhu, Y. Yang, X. Mu, W. Wang, Z. Yao, and H. Yang, "Study on wear and RCF performance of repaired damage railway wheels: Assessing laser cladding to repair local defects on wheels," *Wear*, vol. 430–431, no. March, pp. 126–136, 2019, doi: 10.1016/j.wear.2019.04.028.

[27] W. J. Qian, Z. Q. Huang, H. Ouyang, G. X. Chen, and H. J. Yang, "Numerical investigation of the effects of rail vibration absorbers on wear behaviour of rail surface," *Proc. Inst. Mech. Eng. Part J J. Eng. Tribol.*, vol. 233, no. 3, pp. 424–438, 2019, doi: 10.1177/1350650118785061.

[28] P. F. Borowski, "Digitization, Digital Twins, Blockchain, and Industry 4.0 as Elements of Management Process in Enterprises in the Energy Sector," *Energies*, vol. 14, no. 7, 2021, doi: 10.3390/en14071885.

[29] P. Taylor and A. Johansson, "Vehicle System Dynamics : International Journal of Vehicle Mechanics and Out-of-round railway wheels — a study of wheel polygonalization through simulation of three-dimensional wheel – rail interaction and wear," no. April 2013, pp. 37–41.

